Journal of Molecular Spectroscopy 380 (2021) 111506

Contents lists available at ScienceDirect

Journal of Molecular Spectroscopy

journal homepage: www.elsevier.com/locate/yjmsp

# Threshold photoelectron spectroscopy and density functional theory studies on the $CF_2Cl_2$ ionization energies towards the $B^2B_1$ and $C^2A_1$ ionic states

Baokun Shan [a], Hanhui Zhang [a], Tongpo Yu [a], Yan Chen [a], Xiangkun Wu [b], Xiaoguo Zhou [a,*], Shilin Liu [a]

[a] Hefei National Laboratory for Physical Sciences at the Microscale, Department of Chemical Physics, University of Science and Technology of China, Hefei 230026, China

[b] Paul Scherrer Institute, 5232 Villigen, Switzerland

A B S T R A C T

Threshold photoelectron spectroscopy and density functional theory calculations were performed on dichlorodifluoromethane ($CF_2Cl_2$) in the photon energy range of 11.70–13.90 eV. Using optimized geometries and vibrational frequencies of the $CF_2Cl_2$ neutral and the corresponding cation in the $B^2B_1$ and $C^2A_1$ states at the ωB97XD/aug-cc-pVTZ level of theory, the Franck-Condon factor simulation was conducted for these two bands. According to the great agreement between experimental and simulated spectra, the observed vibrational progressions of the $B^2B_1$ band was reliably assigned, where the 0–0 transition band indicated a precise adiabatic ionization energy (AIE) towards the $B^2B_1$ ionic state of 13.150 ± 0.005 eV. The three symmetric vibrational frequencies of $B^2B_1$ were determined to be $\nu_1^+$ = 1170 $cm^{-1}$, $\nu_2^+$ = 645 $cm^{-1}$, and $\nu_4^+$ = 242 $cm^{-1}$, respectively. Similarly, the AIE towards the $C^2A_1$ ionic state was suggested to be 13.340 eV, based on its plausible Franck-Condon simulation.

## 1. Introduction

Dichlorodifluoromethane ($CF_2Cl_2$) has been extensively used in industry as a plasma-etching agent, refrigerant, solvent, aerosol propellant or blowing agent [1–3]. Meanwhile, it has been known as a typical greenhouse gas due to its strong ozone-depleting substance role in the stratosphere[4–7]. Ionization energy (IE) and dissociation dynamics of $CF_2Cl_2$ are necessary to in-depth understand the whole ion chemistry of various fluorocarbons and its potential applications in the atmosphere [8–10]. However, there is a lack of information on the structure and fundamental parameters of $CF_2Cl_2$ cation relative to its neutral, especially the electronically excited states.

Based on the [core]$(7b_2)^2(12a_1)^2(6b_1)^2(3a_2)^2(8b_2)^2$ electron configuration of neutral $CF_2Cl_2$ molecule [11], the five lowest-lying electronic states of $CF_2Cl_2^+$ cation are $X^2B_2$, $A^2A_2$, $B^2B_1$, $C^2A_1$, and $D^2B_2$ state, respectively [12]. In the past decades, many experimental approaches were applied to measure vertical ionization energies (VIEs) and adiabatic ionization energies (AIEs) of $CF_2Cl_2$ towards these five ionic states, such as photoionization mass spectrometry (PI-MS) [5,6], electron momentum spectroscopy (EMS) [13,14], electron-impact mass spectrometry (EI-MS) [8] and vacuum–ultraviolet (VUV) fluorescence [15]. Most recently, using high-resolution threshold photoelectron spectroscopy (TPES) and theoretical calculations, Zhang *et al.* [16] have obtained a corrected AIE value of 11.565 ± 0.010 eV for the ground state of $CF_2Cl_2^+$ cation, as well as a few vibrational frequencies. This AIE value is obviously smaller than the spectral threshold onset, which had extensively been thought as the AIE. Therefore, this combined method of experimental photoelectron spectra and FC simulation provides a powerful tool to precisely determine AIE [17–20] or electron affinity (EA) values [21–23].

In comparison to the $X^2B_2$ state, the electronically excited states of $CF_2Cl_2^+$ have been much less studied. By measuring photoelectron spectroscopy (PES) using He-I electric discharge lamp, Bunzli *et al.* reported the VIE values of 12.55, 13.13, 13.46, 14.37 eV for the $A^2A_2$, $B^2B_1$, $C^2A_1$, $D^2B_2$ states [24]. Using the same approach, Cvitas *et al.* [25] obtained the approximate VIE results. In addition to these VIE values, Jadrny *et al.* [26] observed vibrational structures of the $B^2B_1$ and $D^2B_2$ states in their photoelectron spectra. Using the peak maximum of the $B^2B_1$ band, they suggested the AIE towards $B^2B_1$ as 13.120 eV. Similarly but with the higher resolution, Pradeep *et al.* [12] confirmed the vibrational progressions of these two states, and gave a cursory assignment. It was worth noting that in their assignment the 0–0 band was located at the low-energy shoulder (13.078 eV as a threshold onset) whereas the peak maximum (13.116 eV) was attributed to be the $X^1A_1(0,0,0,0) \rightarrow B^2B_1(0,0,0,1)$ transition, where only four vibrational modes of $a_1$ symmetry, $(\nu_1^+,\nu_2^+,\nu_3^+,\nu_4^+)$, were excited and the detailed

* Corresponding author.
*E-mail address:* xzhou@ustc.edu.cn (X. Zhou).

https://doi.org/10.1016/j.jms.2021.111506
Received 4 June 2021; Received in revised form 7 July 2021; Accepted 8 July 2021
Available online 14 July 2021

vibrational motions were described in Fig. 3. Thus, they deduced that the AIE values towards $B^2B_1$ and $D^2B_2$ states were 13.078 and 14.126 eV, respectively. The similar spectral structures were observed in Seccombe *et al.*'s TPES but no assignment was given [10]. By calculating molecular structures and harmonic force constant matrix elements of the ground-state $CF_2Cl_2$ neutral and cation in electronically excited states with the self-consistent field (SCF) method, Takeshita *et al.* [27] concluded that the $X^1A_1(0,0,0,0) \rightarrow B^2B_1(0,0,0,0)$ and $X^1A_1(0,0,0,0) \rightarrow B^2B_1(0,0,0,1)$ transitions had the strongest intensities with the approximate energies. In other words, the peak maximum of $B^2B_1$ band in experiment was suggested to be the 0–0 band. Apparently, the identification of the 0–0 transition of $B^2B_1$ band is still controversial in the previous studies. Therefore, our major aim of this work is just to precisely determine AIE for the formation of $CF_2Cl_2^+$ in the $B^2B_1$ and $C^2A_1$ states.

In principle, AIE is defined as the energy difference between neutral and cation after zero-point energy corrections, each at its own optimized geometry, while is also determined as the 0–0 transition energy in experimental TPE spectra. However, some hot bands are probably observed as the threshold onsets in experimental spectra, and furthermore, the 0–0 transition may be too weak to be observed when the molecular geometry is seriously changed in photoionization[17,18,20]. Thus, in this work, the TPES of $CF_2Cl_2^+$ in the $B^2B_1$ and $C^2A_1$ states was re-measured using the threshold photoelectron-photoion coincidence (TPEPICO) double velocity map imaging apparatus at the Hefei Light Source. To assign distinctly vibrational structures, the Franck-Condon (FC) factor simulations have been done with the aid of high-level quantum chemical calculations on optimized geometries and vibrational frequencies of ground-state $CF_2Cl_2$ neutral and cation in the $B^2B_1$ and $C^2A_1$ states. Then, the AIE and VIE values towards these two excited states are reliably determined based on the correct vibrational assignments.

## 2. Experimental and computational methods

The photoionization experiments were performed at the BL09U beamline of the National Synchrotron Radiation Laboratory at Hefei, China, using the TPEPICO velocity map imaging spectrometer. The detailed descriptions of the beamline and configurations of the apparatus have been introduced previously [28], and only a brief overview is given here. The vacuum ultraviolet (VUV) light in the energy range of 11.70–13.90 eV from synchrotron radiation was dispersed by a monochromator, and then passed through a gas filter filled with argon to eliminate high harmonics, as the photoionization light source. The absolute VUV photon energy was calibrated with the well-known ionization energies of argon and krypton. The photon energy resolution ($E/\Delta E$) was about 2000 in the present experiments [29]. A silicon photodiode was used to record photon flux for normalizing ion signal.

A mixture gas (1.2 atm) of $CF_2Cl_2$ (99.99% purity) and helium (1/9 v/v) was injected into the vacuum chamber through a 20-μm-diameter pinhole to form a continuous molecular beam. By collimated with a 0.5-mm-diameter skimmer, the molecular beam intersected with the VUV photons at 10 cm downstream from the nozzle. Under the action of a dc extraction electric field (~15 $V \cdot cm^{-1}$), photoelectrons and photoions were pushed away in opposite directions and projected to position-sensitive detectors with double velocity map imaging. The TPEPICO measurements were performed with a single-start multiple-stop data acquisition mode [30], in which photoelectrons were used to trigger time-of-flight (TOF) measurements of ions. According to the special ion optics, the electron image was remarkably magnified with the delayed flight time. A mask with a 1-mm-diameter hole and a concentric ring was placed in front of the electron detector. Due to the velocity focus effect, the electrons with zero-kinetic energy, usually called as "threshold photoelectrons", together with those energetic electrons with an initial momentum towards the electron detector (so-called "false threshold photoelectrons"), passed through this hole and contributed to TPES. Meanwhile, these energetic electrons with a perpendicular initial momentum would partially pass the ring of the mask, and thus their intensities were used to subtract the TPES contamination contributed by those "false threshold photoelectrons" [31]. This modification approach has been successfully applied recently in dissociative photoionization of many molecules, *e.g.* $NO_2$ [32], $CF_3Cl$ [33], halocyclohexanes [34], fluorocyclohexane [20], and vanillin [35].

Similar to the recent study of $CF_2Cl_2^+$ in ground state [16], density functional theory (DFT) and time-dependent DFT (TD-DFT) were used to calculate optimized geometries and vibrational frequencies of the $CF_2Cl_2$ neutral in ground state and the $CF_2Cl_2^+$ cation in the $B^2B_1$ and $C^2A_1$ states, respectively. A hybrid functional with a dispersion correction approach, ωB97XD [36] with the aug-cc-pVTZ set, was performed as done in the ground state of $CF_2Cl_2^+$ cation [16], in comparison to the previous calculations like HF [27], MRCI [37], CASSCF and CASPT2 [11]. Using the calculated geometries, vibrational frequency and vector of each vibrational mode, and FC factors of the $CF_2Cl_2(X^1A_1) \rightarrow CF_2Cl_2^+(B^2B_1 \text{ or } C^2A_1)$ transitions (defined as the overlapping integral of the vibrational wave functions between initial state and target state) were calculated in a harmonic approximation using the ezSpectrum software [38]. Then, the photoelectron spectra of $CF_2Cl_2^+$ in $B^2B_1$ and $C^2A_1$ states were simulated with a hypothesis of vibrational temperature at 250 K and full width at the half maximum (FWHM) of 25 meV to account for rotational envelope. Based on the well-done spectral simulation, the experimentally observed vibrational progressions were reliably assigned. Therefore, the AIE values towards the $B^2B_1$ and $C^2A_1$ ionic states were precisely determined as the corresponding 0–0 band positions. All the quantum chemical computations were performed with the Gaussian 16 A.03 program package [39].

## 3. Results and discussion

### 3.1. Threshold photoelectron spectrum of $CF_2Cl_2$

Fig. 1 shows the experimental TPES of $CF_2Cl_2$ in the photon energy range of 11.70–13.90 eV, with a step of 5 meV. Four resonance bands are observed and attributed to the photoionization transitions of $CF_2Cl_2$ towards the $X^2B_2$, $A^2A_2$, $B^2B_1$, and $C^2A_1$ ionic states, respectively, referring to the previous studies [12,24–26]. After being normalized with the photon flux, our spectrum is in general agreement with the previous He-I photoelectron spectra [12,24–26], regardless of resonance energies and relative intensities. Thanks to the better vibrational resolution at the rising edge, we have successfully analyzed the first two electronic states, $X^2B_2$ and $A^2A_2$ recently, and an accurate AIE towards the $X^2B_2$ state (11.565 eV) has been achieved from the FC factor simulation [16].

In comparison to the previous photoelectron spectra [12,25], the

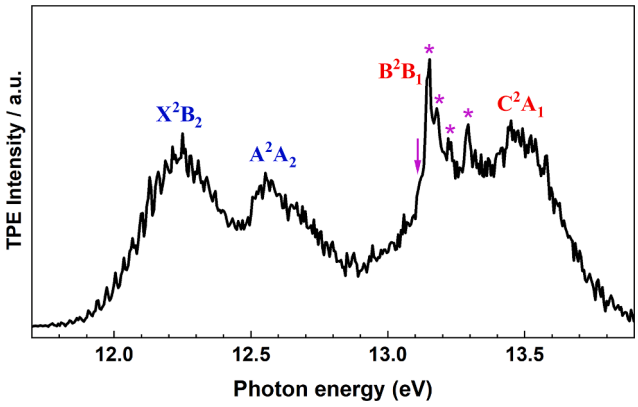


**Fig. 1.** Threshold photoelectron spectrum of $CF_2Cl_2$ in the photon energy range of 11.70–13.90 eV, with a step size of 5 meV. The corresponding electronic states of $CF_2Cl_2^+$ are labeled, and several distinct vibrational peaks of the $B^2B_1$ band are noted with stars, while a weak shoulder peak is marked with an arrow.

spectral intensity in the FC gap between the $A^2A_2$ and $B^2B_1$ states is non-zero (Fig. 1). It is well-known that under the action of one photon with fixed energy like He-I light, the self-ionization of neutral Rydberg states is excluded from photoelectron spectra. Thus, the non-zero baseline of present TPES in this FC gap is contributed by the self-ionization of Rydberg states. From 12.90 eV, the TPE intensity gradually increases, indicative of the formation of the second electronically excited state, $B^2B_1$. It is worth noting that a few vibrational peaks can be distinctly identified below 13.38 eV and noted with stars in Fig. 1, while there is no clear vibrational structure observed for the $C^2A_1$ state spanning from 13.38 to 13.90 eV. Moreover, a weak shoulder peak at 13.120 eV with an arrow is also observed just slightly lower than the strongest peak of $B^2B_1$ band (13.150 eV), which generally agrees with the observation of previous spectra [12,26].

Table 1 summaries the reported ionization energies of $CF_2Cl_2$ towards the low-lying ionic electronic states. Apparently, all VIEs are greatly consistent, however, only two works have reported the different AIEs due to inconsistent vibrational assignments. Pradeep *et al.* [12] attributed this shoulder peak to the 0–0 transition of the $B^2B_1$ band, while Jadrny *et al.* [26] preferred the strongest peak, and assigned this shoulder peak as a hot band. In fact, these previous assignments were arbitrarily achieved only according to energy intervals. Therefore, a reliable vibrational assignment for the $B^2B_1$ band is necessary to precisely determine its AIE value. In addition, due to the overlapping by the $B^2B_1$ band, the $C^2A_1$ band does not show a distinct threshold onset in Fig. 1. Thus, its AIE value (*i.e.* the 0–0 transition) is impossible to be determined without a spectral simulation.

### 3.2. Geometries and frequencies of $CF_2Cl_2^+$ in the $B^2B_1$ and $C^2A_1$ states

In FC photoionization, $CF_2Cl_2$ is kept as the $C_{2V}$ symmetry regardless of the $B^2B_1$ and $C^2A_1$ ionic states. Optimized geometries of the $CF_2Cl_2$ neutral and the corresponding cation in the $B^2B_1$ and $C^2A_1$ states at the ωB97XD/aug-cc-pVTZ level are summarized in Table 2, as well as the previously calculated parameters using HF/MIDI-4 [37], CASPT2/ANO-L and CASSCF/ANO-L methods [11]. As confirmed by our recent calculations of the $CF_2Cl_2(X^1A_1) \rightarrow CF_2Cl_2^+(X^2B_2)$ transition [16], the ωB97XD/aug-cc-pVTZ level was reliable enough to compute structure and vibrational frequencies of the ground-state $CF_2Cl_2^+$ cation. Not only these, all optimized structures of the $CF_2Cl_2$ neutral and cation in Table 1 also generally agree well at the DFT and CASPT2 levels. Thus, the ωB97XD/aug-cc-pVTZ level of theory is subsequently used to calculate harmonic vibrational frequencies and the corresponding vectors.

Unlike the significant geometrical changes upon photoionization to the ionic ground state ($X^2B_2$) [16], only a few variations can be observed for molecular structure when being photoionized to the $B^2B_1$ and $C^2A_1$ states. For the $B^2B_1$ state, the C-F bonds are slightly reduced form 1.325 Å in neutral to 1.294 Å in cation with the increased C-Cl bonds (form 1.770 Å to 1.816 Å), and the bond angle Θ(F-C-F) increases from 108.2° in neutral to 113.5° in cation but Θ(Cl-C-Cl) almost remains unchanged. Naturally, the scissoring vibration of the $CCl_2$ group ($\nu_4^+$) might be excited in photoionization to the $B^2B_1$ ionic state. Meanwhile, the excitations of C-F and C-Cl stretching could be involved as well. Moreover, such minor changes connote that the strongest vibrational peak in the $B^2B_1$ band of TPES should be close to the 0–0 transition. It has been further confirmed by the FC factor calculations in Section 3.3. In addition, a geometric variation from neutral to the $C^2A_1$ ionic state is similar to the photoionization to the $B^2B_1$ state. Two longer C-Cl and shorter C-F bond lengths imply the more significant excitations of C-F and C-Cl stretching when being ionized to the $C^2A_1$ state. In other words, the vibrational excitation becomes more complicated with the $CF_2Cl_2^+(C^2A_1)$ formation.

We also calculated the four highest occupied molecular orbitals of the neutral $CF_2Cl_2$ molecule. The $X^2B_2$, $A^2A_2$, $B^2B_1$, and $C^2A_1$ ionic states are produced by removing an electron from these orbitals. It is worth noting that these molecular orbitals are all contributed by the non-bonding orbitals of lone pair electrons of Cl atom, as shown in Fig. 2. However, unlike the HOMO and HOMO-1 for $X^2B_2$ and $A^2A_2$ states, HOMO-2 and HOMO-3 include two non-bonding orbitals with matching phases (Fig. 2) and prefer to form Π-bond-like interaction between two Cl atoms, especially the latter. As a result, Θ(Cl-C-Cl) is almost maintained unchanged although the C-Cl bonds are apparently weakened, regardless of the $B^2B_1$ and $C^2A_1$ states, which agrees with the conclusion of geometry calculations.

To perform the FC factor simulation, the vibrational vectors and frequencies of $CF_2Cl_2^+$ cation in the $B^2B_1$ and $C^2A_1$ states were calculated respectively. According to the selection rule, only vibrational modes of $a_1$ symmetry might be excited in photoionization [12,26,27]. To be consistent with the previous assignment [26], four total symmetric modes are labeled as $\nu_1^+$ to $\nu_4^+$, and their experimental and calculated values are summarized in Table 3 for comparison. As shown in Fig. 3, both $\nu_1^+$ and $\nu_2^+$ modes are mainly contributed by the motion of carbon atom along the $C_{2v}$ symmetric axis, and the difference is that they are combined with the C-F bond symmetric stretching and the F-C-F scissoring, respectively. The $\nu_3^+$ mode is a synergetic motion of the F-C-F scissoring and the C-Cl stretching, while the $\nu_4^+$ mode is mainly attributed to the Cl-C-Cl scissoring.

As shown in Table 3, the HF/MIDI-4 frequencies are apparently overestimated, compared with the other two methods, but the ωB97XD and CASSCF/ANO-L data are consistent. However, the $\nu_4^+$ frequency of 306 $cm^{-1}$ for $B^2B_1$ suggested by Pradeep *et al.*'s photoelectron spectra [12] is much larger than all calculated values, implying that their

**Table 1**
Vertical ionization energies (VIEs, eV) and adiabatic ionization energies (AIEs, eV) of $CF_2Cl_2$ reported in experiments.

| | Method | $X^2B_2$ | $A^2A_2$ | $B^2B_1$ | $C^2A_1$ | $D^2B_2$ |
|---|---|---|---|---|---|---|
| **VIEs** | | | | | | |
| Turner *et al.* [40] | PES | 12.3 | 12.6 | 13.2 | 13.5 | 14.4 |
| Bunzli *et al.* [24] | PES | 12.27 | 12.55 | 13.13 | 13.46 | 14.37 |
| Cvitas *et al.* [25] | PES | 12.26 | 12.53 | 13.11 | 13.45 | 14.36 |
| Jadrny *et al.* [26] | PES | 12.24 | 12.54 | 13.120 | 13.47 | 14.353 |
| Seccombe *et al.* [10] | TPES | 12.28 | 12.55 | 13.14 | 13.45 | 14.41 |
| Our work | TPES | 12.250 | 12.550 | 13.150 | 13.450 | – |
| **AIEs** | | | | | | |
| Jadrny *et al.* [26] | PES | – | – | 13.120 | – | 14.123 |
| Pradeep *et al.* [12] | PES | 11.734 | – | 13.078 | – | 14.126 |
| Our work | TPES | 11.565[a] | – | 13.150 | 13.340 | – |

[a] . from Ref.[16]

**Table 2**
Optimized geometrical parameters of the neutral $CF_2Cl_2$ and the corresponding cation in the $B^2B_1$ and $C^2A_1$ states calculated at different levels of theory, where the bond length (R) is in unit of Å and the bond angle (Θ) is in degree.

| | ωB97XD | HF [27] | CASSCF [11] | CASPT2 [11] |
|---|---|---|---|---|
| **$CF_2Cl_2(X^1A_1)$** | | | | |
| R(C-F) | 1.325 | 1.309 | – | 1.330 |
| R(C-Cl) | 1.770 | 1.759 | – | 1.755 |
| Θ(F-C-F) | 108.2 | 108.0 | – | 108.0 |
| Θ(Cl-C-Cl) | 111.4 | 111.7 | – | 111.7 |
| **$CF_2Cl_2^+(B^2B_1)$** | | | | |
| R(C-F) | 1.294 | 1.277 | 1.287 | 1.295 |
| R(C-Cl) | 1.816 | 1.807 | 1.892 | 1.827 |
| Θ(F-C-F) | 113.5 | 113.3 | 112.7 | 113.7 |
| Θ(Cl-C-Cl) | 111.8 | 111.4 | 109.7 | 113.2 |
| **$CF_2Cl_2^+(C^2A_1)$** | | | | |
| R(C-F) | 1.289 | 1.281 | 1.282 | 1.295 |
| R(C-Cl) | 1.874 | 1.819 | 1.864 | 1.850 |
| Θ(F-C-F) | 112.8 | 112.2 | 111.5 | 112.1 |
| Θ(Cl-C-Cl) | 113.0 | 113.7 | 113.7 | 114.5 |

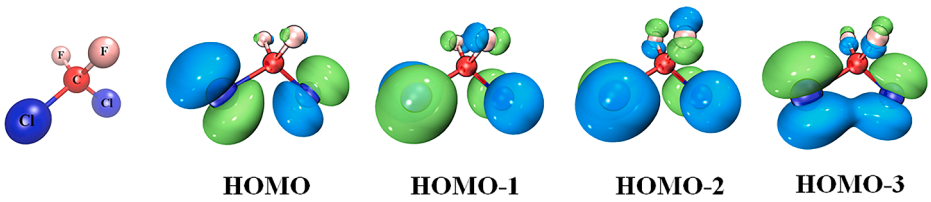


**Fig. 2.** The HOMO, HOMO-1, HOMO-2, HOMO-3 orbitals of neutral $CF_2Cl_2$.

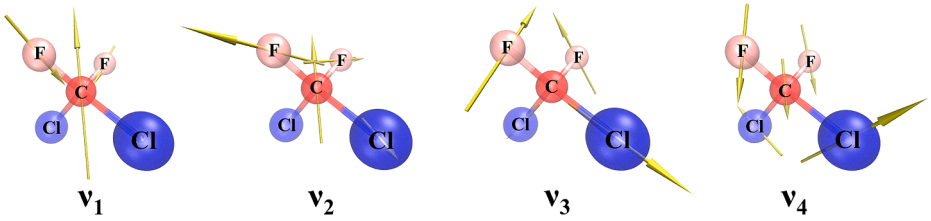


**Fig. 3.** Four total symmetric vibrational modes of the $CF_2Cl_2^+$ cation, where the yellow arrows represent the vibrational displacement vectors of atoms.

**Table 3**
Vibrational frequencies ($cm^{-1}$) of the total symmetric vibrational modes for the $B^2B_1$ and $C^2A_1$ state of $CF_2Cl_2^+$ cation, calculated at the different quantum chemical levels of theory, comparing to the experiment measurement.

| Mode | Theo. | | | Expt. | | |
|---|---|---|---|---|---|---|
| | ωB97XD | HF [27] | CASSCF [11] | PES [12] | PES [26] | TPES [a] |
| **$B^2B_1$** | | | | | | |
| $\nu_1^+$ | 1145 | 1271 | 1172 | – | 1097 | 1170 |
| $\nu_2^+$ | 651 | 712 | 649 | – | 565 | 645 |
| $\nu_3^+$ | 412 | 454 | 350 | – | – | – |
| $\nu_4^+$ | 255 | 276 | 233 | 306 | 210 | 242 |
| **$C^2A_1$** | | | | | | |
| $\nu_1^+$ | 1150 | 1253 | 1212 | – | – | – |
| $\nu_2^+$ | 648 | 702 | 680 | – | – | – |
| $\nu_3^+$ | 369 | 453 | 394 | – | – | – |
| $\nu_4^+$ | 237 | 282 | 248 | – | – | – |

[a] . the present TPES measurement.

assignments were arbitrary due to insufficient vibrational resolution. Thanks to the more distinct vibrational peaks of $B^2B_1$ band in the present TPES, the vibrational frequencies could be reliably determined with the aid of a credible spectral assignment. In Fig. 1, the observed energy intervals between the peaks with stars around the band origin are 1170, 645 and 242 $cm^{-1}$, respectively. To our surprise, these values are close to those calculated frequencies for $\nu_1^+$, $\nu_2^+$, and $\nu_4^+$ vibrational modes for the $B^2B_1$ ionic state at the ωB97XD level, indicative of their spectral contributions, which are confirmed by the FC simulations in Section 3.3. In addition, the vibrational frequencies of $\nu_1^+$ to $\nu_4^+$ modes for $C^2A_1$ state are close to those of $B^2B_1$ owing to their approximate geometries. However, according to its unresolved vibrational structure in Fig. 1, we cannot infer any vibrational assignment for this band.

### 3.3. Franck-Condon factor simulated TPE spectra

Using the optimized geometries and the vibrational frequencies of $CF_2Cl_2$ neutral and cation at the ωB97XD level, the FC factors of the $CF_2Cl_2$ ($X^1A_1$) → $CF_2Cl_2^+$($B^2B_1/C^2A_1$) transitions were calculated. The temperature was adjusted from 20 to 300 K, in order to get best simulation. The max vibrational quantum of the neutral ground state was set as 5 to account for probable hot band excitations. Table 4 lists the calculated major vibrational excitations in the formation of $CF_2Cl_2^+(B^2B_1)$, including peak positions (after an energy shift according to the systemic error of the calculation level in excitation energy), FC factors, spectral intensities (calculated as the product of FC factor and thermal population at 250 K), and vibrational assignments, where those weak transitions (the calculated transition intensity is smaller than 0.010) are ignored from Table 4 in order to simplify discussions.

**Table 4**
Major vibrational peak positions of the simulated TPE spectra in the $B^2B_1$ band range, together with Franck-Condon factors (FCFs) and intensities.

| Peak position /eV [a] | FCF | Intensity | Assignment |
|---|---|---|---|
| | | | $X^1A_1(\nu_{1\text{-}4})$ → $B^2B_1$ ($\nu_{1\text{-}4}^+$) |
| 13.118 | −0.408 | 0.014 | (0,0,0,2) → (0,0,0,1) |
| 13.119 | −0.397 | 0.045 | (0,0,0,1) → (0,0,0,0) |
| 13.147 | 0.519 | 0.030 | (0,0,1,0) → (0,0,1,0) |
| 13.152 | 0.255 | 0.019 | (0,0,0,1) → (0,0,0,1) |
| 13.153 | 0.547 | 0.299 | (0,0,0,0) → (0,0,0,0) |
| 13.180 | 0.381 | 0.016 | (0,0,1,0) → (0,0,1,1) |
| 13.184 | 0.364 | 0.011 | (0,0,0,2) → (0,0,0,3) |
| 13.185 | 0.420 | 0.051 | (0,0,0,1) → (0,0,0,2) |
| 13.186 | 0.402 | 0.162 | (0,0,0,0) → (0,0,0,1) |
| 13.203 | 0.191 | 0.010 | (0,0,0,1) → (0,1,0,0) |
| 13.206 | 0.126 | 0.016 | (0,0,0,0) → (0,0,1,0) |
| 13.218 | 0.294 | 0.025 | (0,0,0,1) → (0,0,0,3) |
| 13.219 | 0.204 | 0.042 | (0,0,0,0) → (0,0,0,2) |
| 13.237 | −0.263 | 0.069 | (0,0,0,0) → (0,1,0,0) |
| 13.267 | 0.234 | 0.016 | (0,0,0,1) → (1,0,0,0) |
| 13.269 | −0.202 | 0.012 | (0,0,0,1) → (0,1,0,2) |
| 13.270 | −0.194 | 0.037 | (0,0,0,0) → (0,1,0,1) |
| 13.295 | −0.306 | 0.010 | (0,0,1,0) → (1,0,1,0) |
| 13.300 | −0.322 | 0.104 | (0,0,0,0) → (1,0,0,0) |
| 13.333 | −0.248 | 0.018 | (0,0,0,1) → (1,0,0,2) |
| 13.334 | −0.237 | 0.056 | (0,0,0,0) → (1,0,0,1) |
| 13.367 | −0.120 | 0.014 | (0,0,0,0) → (1,0,0,2) |
| 13.385 | 0.155 | 0.024 | (0,0,0,0) → (1,1,0,0) |
| 13.418 | 0.114 | 0.013 | (0,0,0,0) → (1,1,0,1) |
| 13.449 | 0.138 | 0.019 | (0,0,0,0) → (2,0,0,0) |
| 13.482 | 0.101 | 0.010 | (0,0,0,0) → (2,0,0,1) |

[a] . after a shift to higher energy by 0.410 eV.

As indicated in Table 4, the $\nu_4^+$ mode (Cl-C-Cl scissoring) is the most important contributor for the whole $B^2B_1$ band in the TPE spectrum, and the corresponding FC factors gradually decrease with its quantum number, regardless of the sole and combined vibrational progressions. Moreover, the $\nu_1^+$ and $\nu_2^+$ modes are also excited in photoionization to the $B^2B_1$ state. It is worth noting that the 0–0 transition is calculated to have the strongest intensity in the whole $B^2B_1$ band, that is, the peak maximum in TPES should correspond to the 0–0 transition.

To confirm our FC simulation, the calculated and our experimental spectra were directly compared together in Fig. 4a. In fact, an optimized temperature of 250 K was chosen to get the best fitting, which is

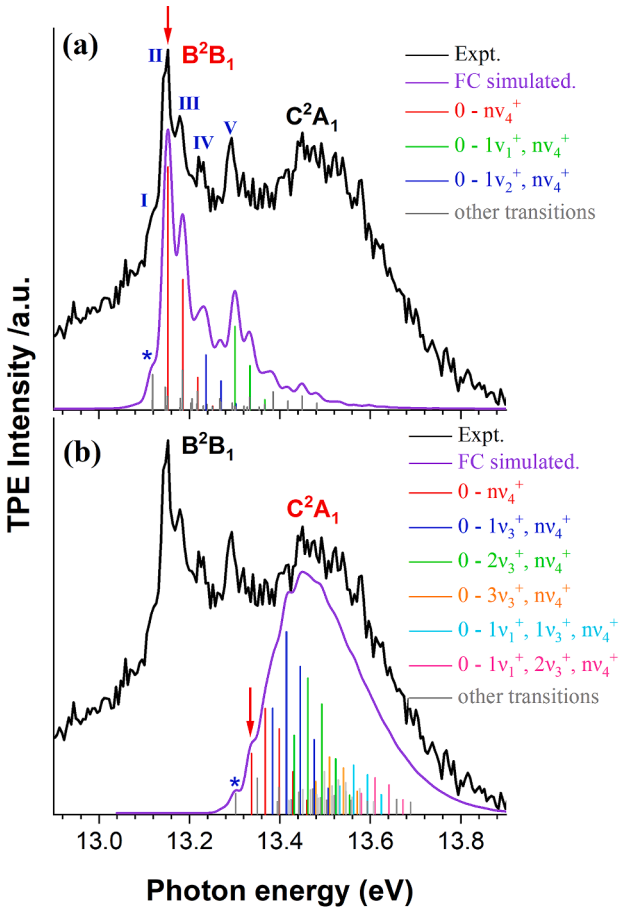


**Fig. 4.** The Franck-Condon simulated and experimental spectra for photoionization from $CF_2Cl_2$ neutral to cation in the $B^2B_1$ and $C^2A_1$ states, where the AIE values of these ionic states are marked in red arrows as well as the major hot bands are pointed out with blue stars, and a FWHM of 25 meV is used in simulation.

consistent with our recent simulation of the ground ionic state [16]. Due to thermal population of initial vibrational levels, a few vibrational progressions including the $\nu_3$ and $\nu_4$ hot bands of neutral $CF_2Cl_2$ might be involved in this TPES. As indicated in Table 4, several hot band transitions have considerable intensities indeed, *e.g.* $X^1A_1(0,0,0,1) \rightarrow B^2B_1(0,0,0,0)$, $X^1A_1(0,0,0,1) \rightarrow B^2B_1(0,0,0,2)$, and $X^1A_1(0,0,1,0) \rightarrow B^2B_1(0,0,1,0)$. Overall, the vibrational excitations in photoionization towards $CF_2Cl_2^+(B^2B_1)$ are much complicated than the case of $X^2B_2$.

As shown in Fig. 4a, a satisfying FC simulated spectrum was obtained for the $B^2B_1$ band, where a few distinct vibrational peaks could be identified without doubt. The sticks in Fig. 4a clearly show these vibrational progressions. The peak I at 13.120 eV is the beginning of a hot band series of $X^1A_1(0,0,0,1) \rightarrow B^2B_1(0,0,0,n)$ (n = 0–3), while the peaks II (13.150 eV) and III (13.180 eV) are the first two bands of the transition progression of $X^1A_1(0,0,0,0) \rightarrow B^2B_1(0,0,0,n)$ (n = 0–2). Moreover, the peaks IV (13.230 eV) and V (13.295 eV) are the first bands of the combination transitions of $X^1A_1(0,0,0,0) \rightarrow B^2B_1(0,1,0,n)$ (n = 0–2) and $X^1A_1(0,0,0,0) \rightarrow B^2B_1(1,0,0,n)$ (n = 0–2), respectively. Table 5 lists our FC simulated and experimental peaks of I-V (also marked with stars in Fig. 1), as well as the previous photoelectron spectral data [26]. Therefore, three vibrational frequencies of $B^2B_1$ ionic state can be readily derived from these assignments, *i.e.* $\nu_1^+ = 1170\ cm^{-1}$, $\nu_2^+ = 645\ cm^{-1}$, and $\nu_4^+ = 242\ cm^{-1}$, which are listed in Table 3 and agree very well with our calculated data. In addition, the $\nu_4$ frequency of the neutral $CF_2Cl_2$ is determined to be 274 $cm^{-1}$ from the first hot band at 13.120 eV, which is also in good agreement with the previous results (258–285 $cm^{-1}$) [25–27]. All these agreements provide solid evidences that the present FC simulation is sufficiently plausible.

**Table 5**
The major vibrational peak positions of the experimental and FC simulated TPE spectra in the $B^2B_1$ band range, together with previous assignments.

| Peak | Present | | | Previous | |
|---|---|---|---|---|---|
| | TPES (eV) | Theo. [a] (eV) | Assignment $X^1A_1(\nu_{1\text{-}4}) \rightarrow B^2B_1$ ($\nu_{1\text{-}4}^+$) | PES [26] (eV) | Assignment $X^1A_1(\nu_{1\text{-}4}) \rightarrow B^2B_1$ ($\nu_{1\text{-}4}^+$) |
| I | 13.120 | 13.119 | (0,0,0,1) → (0,0,0,0) | 13.120 | (0,0,0,0) → (0,0,0,0) |
| II | 13.150 | 13.153 | (0,0,0,0) → (0,0,0,0) | 13.146 | (0,0,0,0) → (0,0,0,1) |
| III | 13.180 | 13.186 | (0,0,0,0) → (0,0,0,1) | 13.190 | (0,0,0,0) → (0,1,0,0) |
| IV | 13.230 | 13.228 | (0,0,0,0) → (0,1,0,0) & (0,0,0,0) → (0,0,0,2) | 13.256 | (0,0,0,0) → (1,0,0,0) |
| V | 13.295 | 13.300 | (0,0,0,0) → (1,0,0,0) | 13.282 | (0,0,0,0) → (1,0,0,1) |

[a] calculated at the ωB97XD /aug-cc-pVTZ level after a shift to higher energy by 0.410 eV.

As indicated in Table 5, the present and Jadrny *et al.*'s assignment [26] are controversial due to the different 0–0 band assignments. On the other hand, although Pradeep *et al.* [12] correctly pointed out the dominant vibrational modes of $\nu_1^+$ and $\nu_4^+$ in photoionization to the $B^2B_1$ state, they achieved an obviously smaller AIE value (13.078 eV) due to insufficient spectral resolution. Fortunately, the development of experimental techniques has efficiently improved the resolution of TPES, which, with the aid of theoretical calculations, has continuously provided opportunities for complement and correction of experimental data. Based on the whole band simulation in Fig. 4a, we are highly confident in our conclusions for the $B^2B_1$ state, including its vibrational frequencies and AIE of 13.150 ± 0.005 eV.

Likewise, we also performed FC factor simulation in the energy range of $C^2A_1$, and plotted the experimental and simulated spectra together in Fig. 4b. Although no distinct vibrational structure can be discerned due to overlapping by the high-energy tail of the $B^2B_1$ band, a brief and reliable contribution can be identified according to the well-fitted spectral contour. As predicted by the geometric calculations, more complicated vibrational excitations are observed in photoionization towards the $C^2A_1$ state. This deduction is confirmed by the FC simulations. As shown in Fig. 4b, at least four combined vibrational progressions are involved with the $X^1A_1(0,0,0,0) \rightarrow C^2A_1(0,0,0,n)$ (n = 0–5) transition. Moreover, the intensities of several hot bands from the $X^1A_1(0,0,0,1)$ level of neutral $CF_2Cl_2$ are also considerable. Therefore, the detailed vibrational assignment is meaningless. However, an AIE value of 13.340 eV for the $C^2A_1$ state can be approximately derived from the comparison between the experimental and simulated spectra. Since the FC simulation at the ωB97XD level shows a great agreement with the experimental data of the $B^2B_1$ band, its performance on the $C^2A_1$ band can be trusted, and thus, the AIE value of $C^2A_1$ is within an energy uncertainty of 0.015 eV (as thrice error as the instrumental resolution) according to the peak maximum in TPE spectrum.

## 4. Conclusions

In this work, we measured the TPES of $CF_2Cl_2$ in the 11.70–13.90 eV photon energy range, where four lowest electronic states of the $CF_2Cl_2^+$ cation, $X^2B_2$, $A^2A_2$, $B^2B_1$, and $C^2A_1$, were involved. The $B^2B_1$ band is observed with some distinct vibrational structures, while no vibrational peaks can be discernible for the $C^2A_1$ band partly due to the overlap of the $B^2B_1$ high-energy tail. To achieve precise determination of AIEs towards these electronic states, the reliable vibrational assignments for these two bands are necessary. Thus, DFT calculations at the ωB97XD/aug-cc-pVTZ level were performed to obtain optimized geometries,

HOMO orbitals, and vibrational frequencies of the neutral $CF_2Cl_2$ and the corresponding cation in the $B^2B_1$ and $C^2A_1$ states. The FC factors for the $CF_2Cl_2(X^1A_1) \rightarrow CF_2Cl_2^+(B^2B_1$ or $C^2A_1)$ transitions were then calculated to simulate vibrational structures of TPES. Based on the well-simulated spectra, the distinct vibrational structures of the $B^2B_1$ band observed in experiment were reliably assigned. Therefore, the AIE towards the $B^2B_1$ ionic state was precisely determined to be 13.150 ± 0.005 eV as the 0–0 transition energy, as well as a few vibrational frequencies of $\nu_1^+ = 1170\ cm^{-1}$, $\nu_2^+ = 645\ cm^{-1}$, and $\nu_4^+ = 242\ cm^{-1}$. Similarly, the AIE towards the $C^2A_1$ ionic state was suggested to be 13.340 eV approximately according to its plausible FC simulation, although no discernible vibrational structure was identified.

## CRediT authorship contribution statement

**Baokun Shan:** Data curation, Formal analysis, Writing - original draft. **Hanhui Zhang:** Investigation, Visualization. **Tongpo Yu:** . **Yan Chen:** . **Xiangkun Wu:** Methodology. **Xiaoguo Zhou:** Conceptualization, Writing - review & editing, Supervision, Funding acquisition. **Shilin Liu:** Supervision, Funding acquisition.

## Declaration of Competing Interest

The authors declare that they have no known competing financial interests or personal relationships that could have appeared to influence the work reported in this paper.

## Acknowledgement

This work was financially supported by the National Key Research and Development program of China (No. 2016YFF0200502), and the National Natural Science Foundation of China (No. 21903079 and 21873089). X. Zhou also thanks the USTC-NSRL Association for financial support.

## References

[1] S. Solomon, Stratospheric ozone depletion: A review of concepts and history, Rev. Geophys. 37 (3) (1999) 275–316.
[2] B.J. Finlayson-Pitts, J.N. Pitts Jr, Chemistry of the upper and lower atmosphere: theory, experiments, and applications, Elsevier, 1999.
[3] D.J. Jacob, Introduction to atmospheric chemistry, Princeton University Press, 1999.
[4] M.J. Molina, F.S. Rowland, Stratospheric sink for chlorofluoromethanes: chlorine atom-catalysed destruction of ozone, Nature 249 (5460) (1974) 810–812.
[5] H.W. Jochims, W. Lohr, H. Baumgärtel, Photoreactions of small organic molecules V. Absorption-, photoion-and resonancephotoelectron-spectra of $CF_3Cl_2$, $CF_2Cl_2$, $CFCl_3$ in the energy range 10–25 eV, Ber. Bunsenges. Phys. Chem. 80 (2) (1976) 130–138.
[6] J.M. Ajello, W.T. Huntress, P. Rayermann, A photoionization mass spectrometer study of $CFCl_3$, $CF_2Cl_2$, and $CF_3Cl$, J. Chem. Phys. 64 (11) (1976) 4746–4754.
[7] H. Schenk, H. Oertel, H. Baumgärtel, Photoreactions of small organic molecules VII photoionization studies on the ion-pair formation of the fluorochloromethanes $CF_2Cl_2$, $CF_3Cl$, and $CFCl_3$, Ber. Bunsenges. Phys. Chem. 83 (7) (1979) 683–691.
[8] R.F. Baker, J.T. Tate, Ionization and dissociation by electron impacf in $CCl_2F_2$ and in $CCl_4$ vapor, Phys. Rev. 53 (1938) 683.
[9] X. Wu, G. Tang, H. Zhang, X. Zhou, S. Liu, F. Liu, L. Sheng, B. Yan, Cl-Loss dynamics in the dissociative photoionization of $CF_3Cl$ with threshold photoelectron–photoion coincidence imaging, Phys. Chem. Chem. Phys. 20 (7) (2018) 4917–4925.
[10] D.P. Seccombe, R.P. Tuckett, B.O. Fisher, Fragmentation of the valence states of $CF_2Cl_2^+$, $CF_2H_2^+$, and $CF_2Br^{2}+$ studied by threshold photoelectron–photoion coincidence spectroscopy, J. Chem. Phys. 114 (9) (2001) 4074–4088.
[11] T. Liu, M.-B. Huang, H.-W. Xi, CASPT2 study on electronic states of the dichlorodifluoromethane cation, Chem. Phys. 332 (2-3) (2007) 277–283.
[12] T. Pradeep, D.A. Shirley, High resolution photoelectron spectroscopy of $CH_2F_2$, $CH_2Cl_2$ and $CF_2Cl_2$ using supersonic molecular beams, J. Electron Spectrosc. Relat. Phenom. 66 (1-2) (1993) 125–138.
[13] N. Chuan-Gang, R. Xue-Guang, D. Jing-Kang, S.u. Guo-Lin, Z. Shu-Feng, H. Feng, L. i. Gui-Qin, Investigation of outer valence orbital of $CF_2Cl_2$ by a new type of electron momentum spectrometer, Chin. Phys. 14 (12) (2005) 2467–2473.
[14] X. Shan, X.J. Chen, L.X. Zhou, Z.J. Li, T. Liu, X.X. Xue, K.Z. Xu, High resolution electron momentum spectroscopy of dichlorodifluoromethane: Unambiguous assignments of outer valence molecular orbitals, J. Chem. Phys. 125 (15) (2006), 154307.
[15] D.P. Seccombe, R.Y.L. Chim, R.P. Tuckett, H.W. Jochims, H. Baumgärtel, Vacuum–ultraviolet absorption and fluorescence spectroscopy of $CF_2H_2$, $CF_2Cl_2$, and $CF_2Br$ 2 in the range 8–22 eV, J. Chem. Phys. 114 (9) (2001) 4058–4073.
[16] H.H. Zhang, T.P. Yu, X.K. Wu, Y. Chen, B.K. Shan, X.G. Zhou, X.H. Dai, S.L. Liu, Ionization energy and thermochemistry of $CF_2Cl_2$ determined from threshold photoelectron spectroscopy, Chem. Phys. Lett. 774 (2021), 138631.
[17] Y. Chen, T.P. Yu, X.K. Wu, X.G. Zhou, S.L. Liu, F.Y. Liu, X.H. Dai, C-F and C-H bond cleavage mechanisms of trifluoromethane ions in low-lying electronic states: Threshold photoelectron-photoion coincidence imaging and theoretical investigations, Phys. Chem. Chem. Phys. 22 (24) (2020) 13808–13817.
[18] T.P. Yu, X.K. Wu, X.G. Zhou, A. Bodi, P. Hemberger, Hydrogen migration as a potential driving force in the thermal decomposition of dimethoxymethane: New insights from pyrolysis imaging photoelectron photoion coincidence spectroscopy and computations, Combust. Flame. 222 (2020) 123–132.
[19] X. Wu, X. Zhou, P. Hemberger, A. Bodi, Conformers, electronic states, and diabolical conical intersections in the valence photoelectron spectroscopy of halocyclohexanes, J. Chem. Phys. 153 (5) (2020) 054305, https://doi.org/10.1063/5.0018293.
[20] X.K. Wu, X.G. Zhou, P. Hemberger, A. Bodi, A guinea pig for conformer selectivity and mechanistic insights into dissociative ionization by photoelectron photoion coincidence: Fluorocyclohexane, Phys. Chem. Chem. Phys. 22 (4) (2020) 2351–2360.
[21] L. Wang, J. Han, Q.Q. Yuan, W.J. Cao, X.G. Zhou, S.L. Liu, X.B. Wang, Electron affinity and electronic structure of hexafluoroacetone (HFA) revealed by photodetaching the [HFA] (center dot) (-) Radical Anion, J. Phys. Chem. A. 125 (3) (2021) 746–753.
[22] L. Wang, Q.Q. Yuan, W.J. Cao, J. Han, X.G. Zhou, S.L. Liu, X.B. Wang, Probing orientation-specific charge-dipole interactions between hexafluoroisopropanol and halides: A joint photoelectron spectroscopy and theoretical study, J. Phys. Chem. A. 124 (10) (2020) 2036–2045.
[23] H. Zhang, W. Cao, Q. Yuan, L. Wang, X. Zhou, S. Liu, X.-B. Wang, Spectroscopic evidence for intact carbonic acid stabilized by halide anions in the gas phase, Phys. Chem. Chem. Phys. 22 (35) (2020) 19459–19467.
[24] J.C. Bunzli, D.C. Frost, F.G. Herring, C.A. McDowell, Assignment of the doublet states arising from ionization of chlorine lone-pairs in molecules possessing $C_{2v}$ symmetry, J. Electron Spectrosc. Relat. Phenom. 9 (3) (1976) 289–305.
[25] T. Cvitaš, H. Güsten, L. Klasinc, Photoelectron spectra of chlorofluoromethanes, J. Chem. Phys. 67 (6) (1977) 2687–2691.
[26] R. Jadrny, L. Karlsson, L. Mattsson, K. Siegbahn, Valence electron spectra of the chlorofluoromethanes $CF_3Cl$, $CF_2Cl_2$ and $CFCl_3$, Phys. Scr. 16 (5-6) (1977) 235–241.
[27] K. Takeshita, A theoretical study on the lonic states and the photoelectron spectra of dichlorodifluoromethane ($CF_2Cl_2$), J. Mol. Spectrosc. 142 (1) (1990) 1–9.
[28] X. Tang, X. Zhou, M. Niu, S. Liu, J. Sun, X. Shan, F. Liu, L. Sheng, A threshold photoelectron-photoion coincidence spectrometer with double velocity imaging using synchrotron radiation, Rev. Sci. Instrum. 80 (11) (2009) 113101, https://doi.org/10.1063/1.3250872.
[29] S. Wang, R. Kong, X. Shan, Y. Zhang, L. Sheng, Z. Wang, L. Hao, S. Zhou, Performance of the atomic and molecular physics beamline at the National Synchrotron Radiation Laboratory, J. Synchrotron Radiat. 13 (6) (2006) 415–420.
[30] A. Bodi, B. Sztáray, T. Baer, M. Johnson, T. Gerber, Data acquisition schemes for continuous two-particle time-of-flight coincidence experiments, Rev. Sci. Instrum. 78 (8) (2007) 084102, https://doi.org/10.1063/1.2776012.
[31] X.-K. Wu, X.-F. Tang, X.-G. Zhou, S.-L. Liu, Dissociation dynamics of energyselected ions using threshold photoelectron-photoion coincidence velocity imaging, Chin. J. Chem. Phys. 32 (1) (2019) 11–22.
[32] T.P. Yu, X.K. Wu, X.H. Ning, Y. Chen, X.G. Zhou, X.H. Dai, F.Y. Liu, S.L. Liu, Ro-vibrational distribution of $NO^+$ dissociated from $NO_2^+$ ions in the $a^3B_2$ and $b^3A_2$ states: a slow "impulsive" dissociation example revealed from threshold photoelectron-photoion coincidence imaging, J. Phys. Chem. A. 125 (16) (2021) 3316–3326.
[33] X.K. Wu, T.P. Yu, Y. Chen, X.G. Zhou, S.L. Liu, X.H. Dai, F.Y. Liu, L.S. Sheng, Dissociative photoionization of $CF_3Cl$ via the $C^2E$ and $D^2E$ states: competition of the C-F and C-Cl bond cleavages, Phys. Chem. Chem. Phys. 21 (9) (2019) 4998–5005.
[34] X.K. Wu, X.G. Zhou, P. Hemberger, A. Bodi, Dissociative photoionization of chloro-, bromo-, and iodocyclohexane: thermochemistry and the weak C-Br Bond in the cation, J. Phys. Chem. A. 125 (2) (2021) 646–656.
[35] X. Wu, X. Zhou, S. Bjelić, P. Hemberger, A. Bodi, Valence photoionization and energetics of vanillin, a sustainable feedstock candidate, J. Phys. Chem. A. 125 (16) (2021) 3327–3340.
[36] J.D. Chai, M. Head-Gordon, Long-range corrected hybrid density functionals with damped atom–atom dispersion corrections, Phys. Chem. Chem. Phys. 10 (44) (2008) 6615–6620.
[37] M. Lewerenz, B. Nestmann, P.J. Bruna, S.D. Peyerimhoff, The electronic spectrum, photodecomposition and dissociative electron attachment of $CF_2Cl_2$: An ab initio configuration interaction study, J. Mol. Struct. (Thoechem.) 123 (3–4) (1985) 329–342.
[38] V. A. Mozhayskiy, A. I. Krylov, ezSpectrum, http://iopenshell.usc.edu/downloads/ .
[39] M.J. Frisch, G.W. Trucks, H.B. Schlegel, G.E. Scuseria, M.A. Robb, J.R. Cheeseman, G. Scalmani, V. Barone, G.A. Petersson, H. Nakatsuji, et al., Gaussian 16, revision C.01; Gaussian, Inc.: Wallingford, CT, 2016.
[40] D.W. Turner, A.D. Baker, C. Baker and C.R. Brundle, Molectdar Photoelectron Spectroscopy, Philos. Trans. Roy. Sot. London, Ser. A, Mathematical and Physical Sciences. 268 (1184) (1970) 7-31.